Data-Driven Gas Sensing Analysis of Tin-Modified Cadmium Sulfide Thin Films

Nadir Fadhil Habubi[1, 2, 3], Saadi Abdulrazaq Abdul Wahab[4], Muna Ahmed Issa[5], Sami Salman Chiad[1] and Yassin Hasan Kadhim[6]

[1]*Department of Physics, College of Education, Mustansiriyah University, 10052 Baghdad, Iraq*
[2]*Department of Radiation and Sonar Technologies, Alnukhba University College, 10001 Baghdad, Iraq*
[3]*Department of Radiology Techniques, Al-Qalam University College, 36001 Kirkuk, Iraq*
[4]*Department of Medical Instruments Technologies, Alnukhba University College, 10001 Baghdad, Iraq*
[5]*Quality Assurance and Performance Evaluation Department, Mustansiriyah University, 10052 Baghdad, Iraq*
[6]*Department of Optics Techniques, College of Health and Medical Techniques, Al-Mustaqbal University, 51001 Hillah, Iraq*
nadirfadhil@uomustansiriyah.edu.iq, muhannadjadan99@gmail.com, muna.ahmed@uomustansiriyah.edu.iq, dr.sami@uomustansiriyah.edu.iq, yassin.hasan@uomus.edu.iq

Keywords: Cds, Sn, PLD, Thin Film, AFM, Bandgap.

Abstract: This study investigates the effect of increasing the x value in CdS(1-x):Snx on the physical properties of nanostructured thin films synthesized via Pulsed Laser Deposition (PLD). Thin films with (x=0.1, 0.3, and 0.5) were deposited on glass substrates under optimized conditions. X-ray diffraction (XRD) confirmed a cubic zinc-blende structure in all samples, with increasing x leading to larger crystallite size and reduced dislocation density and strain. Atomic force microscopy (AFM) showed that increasing x altered surface morphology, reducing grain size and surface roughness, indicating improved uniformity. Optical analysis revealed decreased transmittance and increased absorbance with a higher x value. The optical band gap narrowed from 2.87 eV (x=0.1) to 2.73 eV (x=0.5), due to the creation of localized energy states. Additionally, both the extinction coefficient and refractive index declined with increasing x. These results confirm that increasing x in (CdS(1-x):Snx) effectively modifies the studied characteristics of the films. Resistance in CdS(1-x):Snx films rises with NO_2 exposure due to surface oxidation. Increasing x in CdS(1-x):Snx films reduces NO_2 sensitivity.

1 INTRODUCTION

CdS is in II-VI semiconductor group, widely studied for its wide direct bandgap, high optical transparency, and strong electron affinity [1]. These features make CdS a promising material for various optoelectronic applications, including LED [2], solar cells [3], gas sensors [4], liquid crystal displays [5], and field-effect transistors [6], [7]. Its excellent optical and electrical properties, combined with its compatibility with different dopants, have increased its research relevance in recent years. Doping CdS with metallic elements such as manganese (Mn) [8], zinc (Zn) [9], nickel (Ni) [10], cerium (Ce) [11], copper (Cu) [12], indium (In) [13], and iron (Fe) [14] significantly alters its structural and electronic properties. Depending on the dopant type and concentration, doping can convert CdS from its natural n-type conductivity to p-type [14]. Typically, Pure CdS exhibits n-type behavior with low resistivity (10^{-2} to 10^{-4} Ω·cm) and high transparency in the visible range [15], making it highly suitable for photovoltaic and optoelectronic devices. CdS thin films have been synthesized using several methods, including thermal evaporation [16], [17], CBD [18], [19], MBE [20], and pulsed laser deposition [21], [22]. Furthermore, due to its excellent film purity, precise control over thickness and stoichiometry, and ability to produce dense, homogeneous coatings suitable for most advanced applications, PLD is considered the most appropriate method. Focuses on the synthesis and study of the properties of $CdS_{(1-x)}:Sn_x$ thin films. It aims to investigate how increasing the x value in $CdS_{(1-x)}:Sn_x$ affects the films' structural, morphological, and optical properties.

2 EXPERIMENTAL

CdS_{1-x} and Sn_x (x = 0.1, 0.3, and 0.5 wt%) were mixed. A gate mortar is also used to mix the powder of the materials for one hour to ensure the homogeneity and adequate cohesion of the samples. This mixture is then fed into a hydraulic press to form pellets (d = 20 mm) at a pressure of 6 Pa for 10 min. For the PLD deposition of thin CdS:Sn films, the glass substrates (75 × 25 × 1.2) mm were used. PLD was carried out in a vacuum chamber with a focusing YAG laser (wavelength 1064 nm, laser energy 400 mJ, peak duration 9 ns, repetition rate 6 Hz) applying 200 laser pulses onto a clean CdS:Sn target. The angle of incidence of the laser pulses at the surface of the target material should be as high as 45° to give the largest area of deposition on the glass base. The glass cylindrical chamber, 30 cm and 40 cm in height, was used for the deposition of thin films at all heights, under pressure (10–2) Torr. Structural properties were analyzed using XRD with a SHIMADZU XRD-6000. Surface morphology was studied by atomic force microscopy (AFM) with an AA3000 SPM. Optical properties, including transmittance and absorbance, were evaluated using a Shimadzu double-beam spectrophotometer. The sensitivity of CdS: Sn gas sensors was assessed based on resistance changes inside a cylindrical chamber measuring 7 × 16 cm.

3 RESULTS AND DISCUSSIONS

Figure 1 presents the X-ray diffraction (XRD) patterns of the synthesized CdS(1−x):Snx thin films, where the diffraction peaks are clearly observed at 2θ values of 28.36°, 36.72°, 51.84°, and 66.81°, corresponding to the (101), (102), (200), and (203) crystallographic planes, respectively. The presence of these well-defined reflections confirms the high crystalline quality of the deposited films, which are consistent with a cubic zinc-blende structure as referenced in JCPDS card No. 43-0985. The dominant intensity of the (101) peak indicates a preferred growth orientation along this direction, suggesting enhanced crystallinity and improved grain alignment during film formation [23], [24]. This behavior is in good agreement with previously reported results in the literature [25], [26].

The crystallite size (D) was evaluated using Scherrer's equation [27], [28], where the full width at half maximum and diffraction angle are key parameters. The calculated values are 13.74 nm for x = 0.1, 14.97 nm for x = 0.3, and 15.85 nm for x = 0.5. The gradual increase in crystallite size with increasing Sn content indicates that higher x values promote grain growth. This trend can be attributed to enhanced atomic diffusion and reduced lattice constraints, which facilitate the coalescence of smaller crystallites into larger grains during film formation [29], [30].

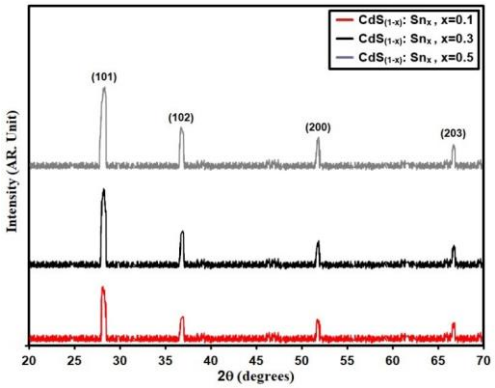

Figure 1: XRD patterns of the deposited films.

The dislocation density (δ) was determined using the standard relation reported in [31], [32], where it is inversely proportional to the square of crystallite size. The results show a decrease in δ from 52.96×10^{14} lines/m² at x = 0.1 to 39.95×10^{14} lines/m² at x = 0.5. This reduction reflects an improvement in crystalline quality, indicating fewer structural defects and dislocations within the lattice. Such behavior is consistent with the observed increase in crystallite size and confirms enhanced structural stability of the films [33], [34].

The lattice strain (ε) was calculated using the relation given in [35], [36]. The obtained values decrease from 25.21×10^{-4} to 21.91×10^{-4} with increasing x value in CdS(1−x):Snx, indicating a progressive relaxation of internal stresses. This reduction in strain is associated with improved crystal ordering and grain growth, which collectively reduce lattice distortions and enhance overall material quality [37], [38]. The complete set of structural parameters, including D, δ, and ε, is summarized in Table 1, while Figure 2 illustrates their variation as a function of composition.

Figure 3 (a1–c1) shows AFM micrographs along with surface morphology analysis of CdS(1−x):Snx thin films. The 3D surface profiles and grain size distribution indicate the formation of nearly spherical nanograins, with the grain size increasing from 47.8 nm at x = 0.1 to 93.4 nm at x = 0.5. This increase suggests improved crystallite ordering and enhanced

grain growth with higher Sn content, leading to a more uniform surface structure [39], [40]. In contrast, surface roughness parameters, including average roughness (Ra) and root mean square roughness (Rrms), show an increasing trend with x. The Ra values increase from 2.42 nm (x = 0.1) to 7.71 nm (x = 0.5), while Rrms values are 3.35 nm, 5.27 nm, and 8.72 nm for x = 0.1, 0.3, and 0.5, respectively. This increase in roughness is attributed to enhanced grain growth and surface restructuring during film deposition, which leads to a more pronounced surface topology [41], [42]. Detailed AFM parameters are provided in Table 2.

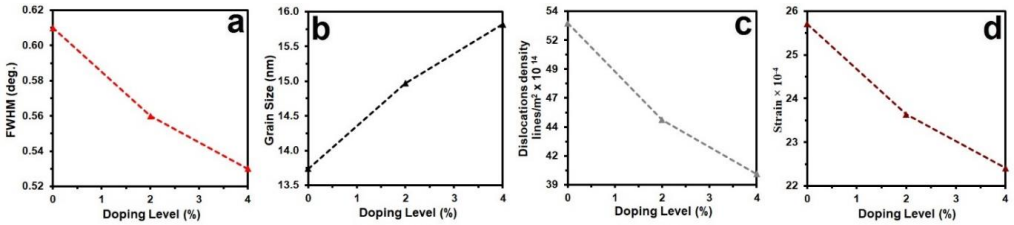

Figure 2: (a) FWHM), (b) Grain size, (c) Dislocation density, and (d) Strain of the deposit films.

Table 1: D, E_g, and structural properties of the deposit films.

Samples	(hkl) Plane	2 θ (°)	FWHM (°)	E_g (eV)	D (nm)	Dislocations density × 10^{14} lines/m	Strain × 10^{-4}
$CdS_{(1-x)}:Sn_x$, x=0.1	101	28.36	0.61	2.87	13.74	52.96	25.21
$CdS_{(1-x)}:Sn_x$, x=0.3	101	28.31	0.56	2.80	14.97	44.62	23.14
$CdS_{(1-x)}:Sn_x$, x=0.5	101	28.27	0.53	2.73	15.82	39.95	21.91

Table 2: Surface morphology parameters obtained from AFM analysis of the deposited films.

Samples	Grain Size (nm)	R_a (nm)	R_{rms} (nm)
$CdS_{(1-x)}:Sn_x$ at x=0.1	47.8	2.42	3.35
$CdS_{(1-x)}:Sn_x$ at x=0.3	69.8	7.32	5.27
$CdS_{(1-x)}:Sn_x$ at x=0.5	93.4	7.71	8.72

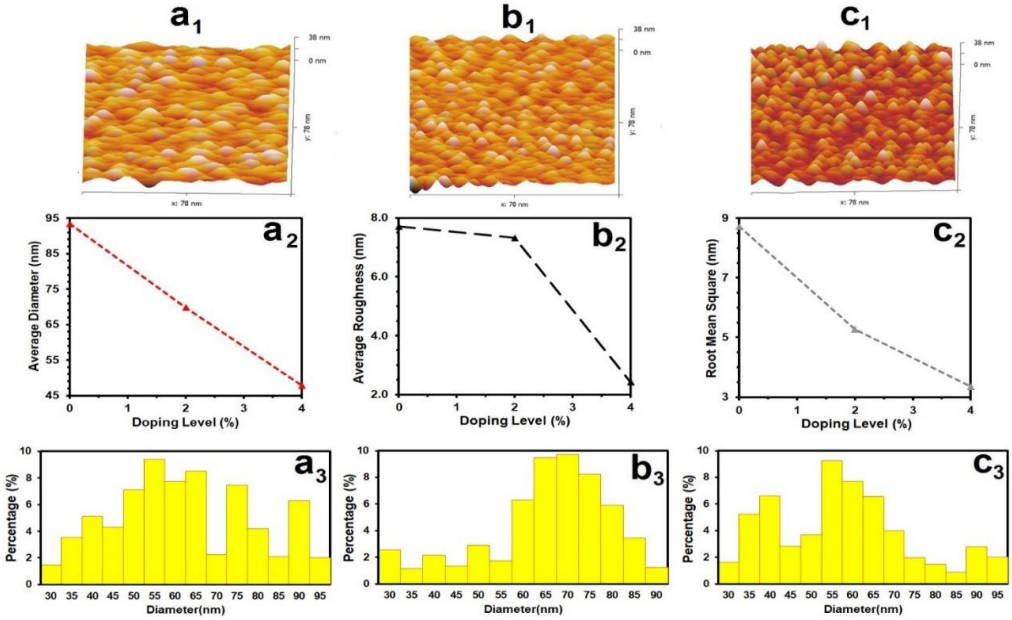

Figure 3: FM micrographs and surface roughness analysis of CdS(1−x):Snx thin films at different Sn concentrations.

Figure 4 illustrates the optical transmittance behavior of CdS(1−x):Snx thin films, showing a clear decreasing trend with increasing x value. This reduction in transmittance can be associated with enhanced optical absorption and increased scattering effects caused by the incorporation of Sn atoms into the CdS lattice. As the Sn content increases, the optical density of the films rises, which leads to a corresponding decrease in transparency. In addition, structural analysis from AFM indicates variations in surface morphology with changing composition, where grain refinement and surface modification contribute to increased light scattering, further reducing the transmitted light intensity. The combined influence of these structural and compositional changes explains the observed decline in optical transmittance with increasing x [43], [44].

The relationship between absorbance (A) and transmittance (T) is described using the standard optical expression reported in [45], [46], where transmitted and incident light intensities are considered. The optical absorbance spectra of CdS(1−x):Snx thin films are presented in Figure 5 over a range of wavelengths. All samples exhibit higher absorbance in the ultraviolet region and comparatively lower absorption in the visible region, which is typical for semiconductor materials where UV absorption is associated with electronic transitions across the band gap. It is also observed that absorbance increases progressively with increasing x across the entire spectral range [47], [48]. This enhancement is likely due to the introduction of defect-related or impurity-induced energy levels within the band gap, which provide additional pathways for electronic transitions and strengthen light–matter interaction. Consequently, higher Sn content modifies the electronic structure and increases the density of states, leading to enhanced optical absorption [49].

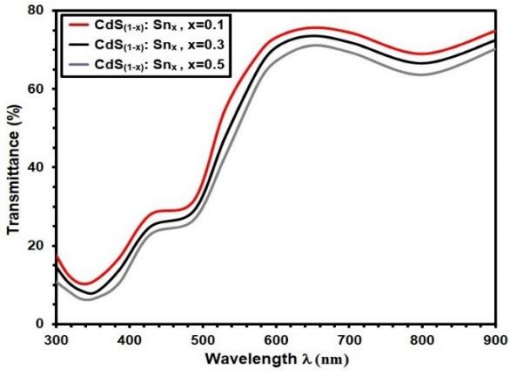

Figure 4: Transmittance of the deposit films.

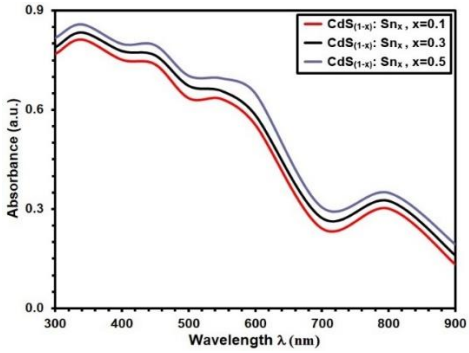

Figure 5: Absorbance of $CdS_{(1-x)}$-Sn_x films.

The absorption coefficient (α) was evaluated using the relation reported in [50], [51], which links absorbance with film thickness. The variation of α with photon energy (hν) is presented in Figure 6. The results indicate that all films exhibit high absorption coefficients exceeding 10^4 cm^{-1}, confirming strong optical absorption and supporting the presence of direct electronic transitions [37]. A slight increase in α is observed with increasing x value in CdS(1−x):Snx. This behavior can be attributed to the formation of localized energy states within the band structure introduced by Sn incorporation. These defect- or impurity-related states extend the absorption process into lower energy regions, enabling sub-bandgap transitions and shifting the absorption edge toward lower photon energies, which ultimately enhances the overall absorption coefficient [52].

The optical bandgap (Eg) was determined using Tauc's relation as described in [53], [54]. The corresponding plots are shown in Figure 7, which clearly demonstrate a decreasing trend in Eg with increasing x. The bandgap values are found to be 2.87 eV, 2.80 eV, and 2.73 eV for x = 0.1, 0.3, and 0.5, respectively. The relatively higher bandgap at x = 0.1 is attributed to quantum confinement effects associated with nanostructured films, which typically lead to bandgap widening compared to bulk material [55]. The observed decrease in Eg with increasing Sn content is explained by the incorporation of Sn ions into the CdS lattice, either substitutionally or interstitially, which modifies the electronic band structure. The bandgap values are summarized in Table 1, confirming the systematic reduction of Eg with increasing x.

Figure 8 presents the extinction coefficient (k) as a function of wavelength (λ) for all samples. A decreasing trend in k is observed with increasing x value in CdS(1−x):Snx. The highest extinction coefficient is recorded for x = 0.1 (k = 0.76), while

lower values are obtained for x = 0.3 (0.743) and x = 0.5 (0.721). This trend indicates that increasing Sn content leads to reduced optical losses. The decrease in k is directly correlated with the behavior of the absorption coefficient, as both parameters are strongly interrelated. Therefore, the reduction in k with increasing x can be attributed to changes in optical absorption characteristics induced by compositional modification [39].

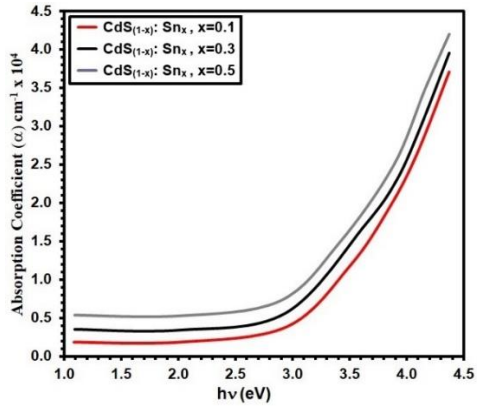

Figure 6: α Vs hν of the $CdS_{(1-x)}:Sn_x$ films.

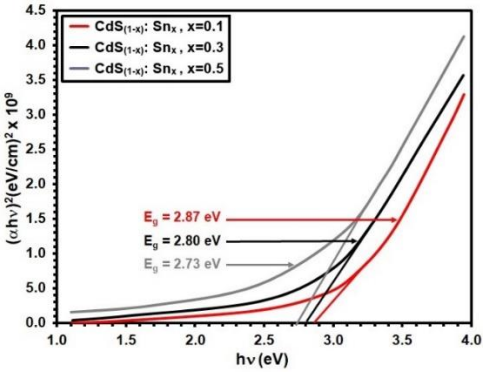

Figure 7: $(\alpha h\nu)^2$ Vs hν of the $CdS_{(1-x)}:Sn_x$ films.

The extinction coefficient (k) was determined using the standard optical relation reported in [56], [57], which relates it to the absorption coefficient and wavelength. The refractive index (n) was then evaluated using the expression given in [58], [59], where reflectivity (R) and extinction coefficient (k) are taken into account.

The variation of refractive index with wavelength is presented in Figure 9. The results show that the film with x = 0.1 exhibits the highest refractive index value of 3.37 at 520 nm, while the lowest value of 3.22 is observed for the film with x = 0.5. For all samples, the refractive index decreases exponentially with increasing wavelength in the range of 600–900 nm, indicating reduced optical interaction and lower losses at longer wavelengths [40]. This behavior suggests improved transparency in the near-infrared region due to reduced absorption and scattering effects.

In addition, the extinction coefficient shows a similar wavelength-dependent trend for all compositions. A gradual decrease in k is observed with increasing x value in CdS(1−x):Snx. This reduction reflects compositional effects on the optical absorption behavior of the films, where higher Sn content modifies the electronic structure and leads to lower optical attenuation [18].

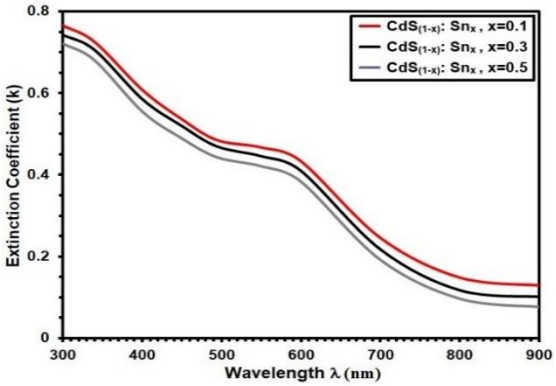

Figure 8: k of the $CdS_{(1-x)}:Sn_x$ films.

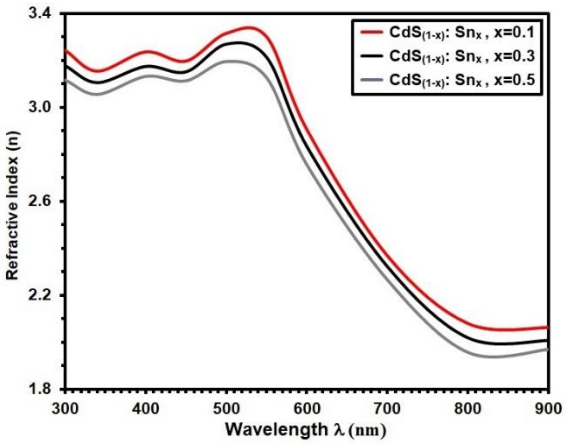

Figure 9: n of the CdS(1-x):Snx films.

Figure 10 illustrates the increase in resistance over time for $CdS_{(1-x)}:Sn_x$ thin films with x=0.1, 0.3, and 0.5 when exposed to 200 ppm NO_2 at 100 °C, indicating surface oxidation during gas exposure [54], [55]. The adsorption of NO_2 molecules on the film surface leads to the removal of O_2^+ ions, releasing electrons into the conduction band and resulting in a rise in resistance. Notably, increasing the x value,

particularly at x=0.5, significantly amplifies this resistance increase, highlighting its strong influence on the films' gas sensing and semiconductor properties [60], [61]. This enhanced resistance response can be explained by the fact that higher x values introduce additional trap states and defects in the $CdS_{(1-x)}:Sn_x$ lattice [62], [63].

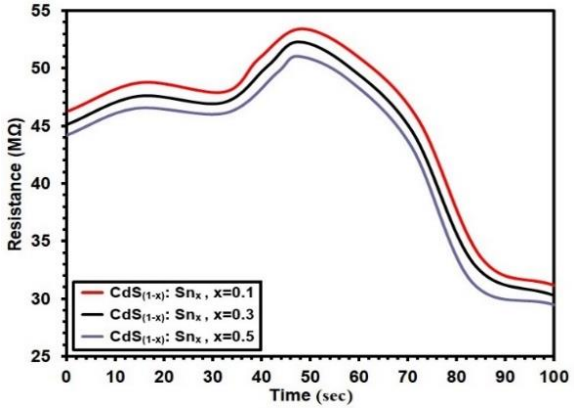

Figure 10: Resistance change over time for CdS(1-x):Snx with x=0.1, 0.3, and 0.5.

Sensitivity (S) was evaluated using the standard expression reported in [64], [65], which describes the relative change in electrical resistance upon exposure to the target gas. In this relation, $R_g$represents the baseline resistance in air, while $R_a$corresponds to the resistance measured under NO_2 exposure.

Figure 11 shows that the sensitivity of CdS(1−x):Snx thin films decreases progressively with increasing x value. This reduction in sensing performance is mainly associated with an increase in electrical resistance and enhanced charge carrier recombination after NO_2 exposure [66], [67]. As the Sn content increases, additional defect- or trap-related states are introduced into the band structure, which facilitate recombination processes and reduce the concentration of free charge carriers available for conduction [68]. As a result, both electrical conductivity and gas sensing response are diminished.

Overall, the observed trend indicates that higher x values negatively affect NO_2 sensing behavior by limiting effective charge transfer processes and reducing the interaction between gas molecules and the film surface, thereby suppressing the overall sensor response [69].

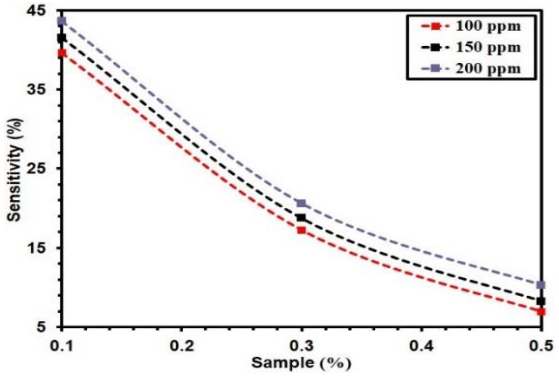

Figure 11: Sensitivity (S) of $CdS_{(1-x)}:Sn_x$ films at x=0.1, 0.3, and 0.5.

4 CONCLUSIONS

Nanostructured $CdS_{(1-x)}:Sn_x$ thin films with x=0.1, 0.3, and 0.5 were synthesized via pulsed laser deposition (PLD). Structural analysis confirmed a cubic zinc-blende phase with improved crystallinity as the x value increased. Crystallite size grew, while dislocation density and strain decreased with higher x. AFM results showed reduced particle size and surface roughness due to increasing x. Optically, higher x values lowered transmittance and raised absorbance. The absorption coefficient increased, and the bandgap narrowed from 2.87 eV (x=0.1) to 2.73 eV (x=0.3), attributed to localized energy levels formed by Sn substituting Cd. Additionally, both the extinction coefficient and refractive index decreased as x increased, reflecting changes in the films' optical properties. Resistance increases over time in $CdS_{(1-x)}:Sn_x$ films exposed to NO_2. Elevated x value in $CdS_{(1-x)}:Sn_x$ films leads to a decrease in NO_2 sensitivity.

ACKNOWLEDGMENTS

The authors express their gratitude for the support provided by Mustansiriyah University (www.uomustansiriyah.edu.iq) and Alnukhba University College.

REFERENCES

[1] H. R. Motinho, D. Albin, Y. Yaan, R. G. Dheo, X. Li, C. Perkis, and C. S. Jiang, "Thin Solid Films 436," pp. 175, 2003.

[2] H. Metin and R. Esen, "Semicond. Sci. Technol. 18," pp. 647, 2003.

[3] G. S. Vorobjov, V. O. Zhurba, and A. S. Krivets, "J. Nano-Electron. Phys. 2 No. 4," pp. 47, 2010.

[4] A. Zeho and J. G. Vazquez Luna, "Sol. Energ. Mater. Sol. C 68," pp. 217, 2001.

[5] J. Levinson, F. R. Shepherd, P. J. Scanlon, W. D. Westwood, G. Este, and M. Rider, "J. Appl. Phys. 53," pp. 1193, 1982.

[6] U. Pal, R. Silva-Gonzalez, G. Martinez-Montes, M. Gracia-Jimenez, M. A. Vidal, and S. Torres, "Thin Solid Films 305," pp. 345, 1997.

[7] J. H. Schon, O. Schenker, and B. Batlogg, "Thin Solid Films 385," pp. 271, 2001.

[8] Z. L. Wang, "Functional oxide nanobelts: materials, properties and potential applications in Nanosystems and biotechnology," Annu. Rev. Phys. Chem., vol. 55, pp. 159–196, 2004.

[9] M. A. Issa and K. A. Aadim, "Study the structural and optical properties of Zinc Oxide prepared by pulse laser deposition," J. Opt., 2024, https://doi.org/10.1007/s12596-024-02034-2.

[10] M. A. Ibrahim, A. R. Ibrahim, and O. Musa, "Investigation of the properties of cadmium sulphide thin films for solar cell applications," Int. J. Energy Eng., vol. 4, no. 3, pp. 61–67, 2014.

[11] T. Chtouki, Y. El Kouari, B. Kulyk, A. Louardi, A. Rmili, H. Erguig, B. Elidrissi, L. Soumahoro, and B. Sahraoui, "Spin-coated nickel doped cadmium sulfide thin films for third harmonic generation applications," J. Alloy Compd., vol. 696, pp. 1292–1297, 2017.

[12] S. Sagadevan and K. Pandurangan, "Synthesis, structural, optical and electrical properties of cadmium sulphide thin films by chemical bath deposition method," Int. J. ChemTech Res., vol. 6, no. 7, pp. 3748–3752, 2014.

[13] Ş. Baturay, "Indium doping on the structural, surface and optical properties of CdS thin films prepared by ultrasonic spray pyrolysis method," J. BAUN Inst. Sci. Technol., vol. 19, no. 2, pp. 264–274, 2017.

[14] N. Hernandez, F. Berrellez, R. Mizquez, O. Ramirez, I. Mejia, and M. Quevedo, "CdS-based p-i-n diodes using indium and copper doped CdS films by pulsed laser deposition," Sci. Technol., vol. 30, no. 6, pp. 065003–065007, 2015.

[15] S. A. Mahmoud, A. A. Ibrahim, and A. S. Riad, "Thin Solid Films 372," pp. 144, 2000.

[16] A. Ashour, N. El-Kadry, and S. A. Mahmoud, "On the electrical and optical properties of CdS films thermally deposited by a modified source," Thin Solid Films, vol. 269, pp. 117–120, 1995.

[17] I. Oliva, O. Solis-Canto, R. Castro-Rodriguez, and P. Quintana, "Thin Solid Films 391," pp. 28, 2001.

[18] D. Barreca, A. Gasparotto, C. Maragno, and E. Tondello, "CVD of nanosized ZnS and CdS thin films from single-source precursors," J. Electrochem. Soc., vol. 151, no. 6, pp. G428–G435, 2004.

[19] Ph. Hofimann, K. Horn, A. M. Bradshaw, R. L. Johnson, D. Fuchs, and M. Cardona, "Phys. Rev. B 47," pp. 1639, 1993.

[20] M. A. Issa and K. A. Aadim, "Optical and structural characterization of ZnO:NiO nanocomposite prepared by pulsed laser deposition method," J. Opt., vol. 54, pp. 2357–2362, 2025, https://doi.org/10.1007/s12596-024-01951-6.

[21] M. A. Issa and K. A. Aadim, "Influence of laser energy on structural and optical properties of ZnO(x):NiO(1−x) films prepared by pulse laser deposition," J. Opt., 2024, https://doi.org/10.1007/s12596-024-02212-2.

[22] F. Chale-Lara, M. Zapata-Torres, M. Melendez-Lira, and H. Peraza-Vazquez, "Optical and structural properties of CdS films grown by CSVT technique," Phys. Status Solidi C, vol. 2, no. 10, pp. 3694–3697, 2005.

[23] H. Shour, F. El Akkad, R. Bohari, and K. H. Herrmann, "Properties of RF sputtered CdS thin films," Proc. 11th Int. Conf. Microelectron., pp. 263–265, 1999.

[24] B.-S. Moon, J.-H. Lee, and H. Jung, "Comparative studies of the properties of CdS films deposited on different substrates by R.F. sputtering," Thin Solid Films, vols. 511–512, pp. 299–303, 2006.

[25] L. S. Ravangave, S. D. Misal, U. V. Biradar, and K. N. Rothod, "Comparative study of structural, morphological and optical characterization of CdS, CdAlS annealed thin films," Mater. Phys. Mech., vol. 14, pp. 129–136, 2012.

[26] N. N. Jandow, N. F. Habubi, S. S. Chiad, I. A. Al-Baidhany, and M. A. Qaeed, "Annealing effects on band tail width, Urbach energy and optical parameters of Fe2O3:Ni thin films," J. Phys.: Conf. Ser., 2020.

[27] M. D. Uplane and S. H. Pawar, "Solid State Commun. 46," pp. 847, 1983.

[28] M. Muthusamy, S. Muthukumaran, and M. Ashokkumar, "Composition dependent optical, structural and photoluminescence behavior of CdS:Al thin films by chemical bath deposition method," Ceram. Int., vol. 40, pp. 10657–10666, 2014.

[29] S. H. Al-Jumaili and N. T. Mahmood, "Structural and optical properties of CdS:In nanoparticles thin films prepared by CBD technique," Int. J. Adv. Innov. Eng. Manag., vol. 2, no. 10, pp. 60–65, 2013.

[30] E. H. Hadi, M. A. Abbsa, A. A. Khadayeir, Z. M. Abood, N. F. Habubi, and S. S. Chiad, "Effects of Mn doping on the characterization of nanostructured TiO2 thin films deposited via chemical spray pyrolysis method," J. Phys.: Conf. Ser., vol. 1664, no. 1, 2020.

[31] T. H. Mubarak, K. H. Hassan, and Z. M. A. Abbas, "Using X-ray diffraction and scanning electron microscope to study zinc oxide nanoparticles prepared by wet chemical method," Adv. Mater. Res., vol. 685, pp. 119–122, 2013.

[32] N. N. Parvathy, G. M. Pajonk, and A. V. Rao, "J. Mater. Synth. Proc. 7," pp. 221, 1999.

[33] R. I. Jasim, E. H. Hadi, S. S. Chiad, N. F. Habubi, and M. Jadan, "Effect of silver-doping on the structural, topography and optical CdSe thin films," J. Ovonic Res., vol. 19, no. 2, pp. 187–196, 2023.

[34] M. H. Albanda Al-Timimi, W. H. Abdullah, and M. Z., "Influence of thickness on some physical characterization for nanostructured MgO thin films," East Eur. J. Phys., vol. 2023, no. 2, pp. 173–181, 2023.

[35] Ray, II-VI Compounds, 1st ed., Printed in Great Britain by Neili and Co. Ltd., Edinburgh, 1969.

[36] Y. Al-Douri, Q. Khasawneh, S. Kiwan, U. Hashim, S. B. Abd Hamid, A. H. Reshak, A. Bouhemadou, M. Ameri, and R. Khenata, "Structural and optical insights to enhance solar cell performance of CdS nanostructures," Energy Convers. Manage., vol. 82, pp. 238–243, 2014.

[37] L. Powlowski, The Science and Engineering of Thermal Spray Coating, 2nd ed., John Wiley & Sons, France, 2007.

[38] K. K. Nanda, S. N. Sarangi, S. Mohanty, and S. N. Sahu, "Thin Solid Films 322," pp. 21–27, 1998.

[39] F. Aghaei, R. Sahraei, E. Soheyli, and A. Daneshfar, "Dopant-concentration dependent optical and structural properties of Cu-doped ZnS thin films," J. Nanostruct., vol. 12, no. 2, pp. 330–342, 2022.

[40] E. U. Masumdar, V. B. Gaikwad, V. B. Pujari, P. D. More, and L. P. Deshmukh, "Some studies on chemically synthesized antimony-doped CdSe thin films," J. Mater. Chem. Phys., vol. 77, pp. 669–676, 2003.

[41] R. B. López-Flores, O. Portillo Moreno, R. Lozada-Morales, and R. Palomino-Merino, "The effect of Er3+ doping on the physical properties of CdSe thin films deposited by chemical bath," Rev. Mex. Fis., vol. 52, pp. 39–41, 2006.

[42] A. M. Perez Gonzalez, I. V. Arreola, and C. S. Tepantlán, "Effects of indium doping on the structural and optical properties of CdSe thin films deposited by chemical bath," Rev. Mex. Fis., vol. 55, pp. 51–54, 2009.

[43] M. A. Mahdi, S. J. Kasem, J. J. Hassen, A. A. Swadi, and S. K. Al-Ani, "Structural and optical properties of chemical deposition CdS thin films," Int. J. Nanoelectron. Mater., vol. 2, pp. 163–172, 2009.

[44] N. F. Habubi, K. H. Abass, S. S. Chiad, D. M. A. Latif, J. N. Nidhal, and A. I. Al Baidhany, "Dispersion parameters of polyvinyl alcohol films doped with Fe," J. Phys.: Conf. Ser., vol. 1003, no. 1, 012094, 2018.

[45] J. Humenberger, G. Linnert, and K. Lischka, "Hot-wall epitaxy of CdS thin films and their photoluminescence," Thin Solid Films, vol. 121, no. 1, pp. 75–83, 1984.

[46] A. J. Haider, A. M. Mousa, and S. M. H. Al-Jawad, "Annealing effect on structural, electrical and optical properties of CdS films prepared by CBD method," J. Semicond. Technol. Sci., vol. 8, pp. 326–332, 2008.

[47] R. R. Pawar, R. A. Bhavsar, and S. G. Sonawane, "Structural and optical properties of chemical bath deposited Ni-doped Cd–Se thin films," Indian J. Phys., vol. 86, pp. 871–876, 2012.

[48] G. Ojeda-Barrero, A. I. Oliva-Avilés, A. I. Oliva, R. D. Maldonado, M. Acosta, and G. M. Alonzo-Medina, "Effect of the substrate temperature on the physical properties of sprayed-CdS films by using a litomatized perfume atomizer," Mater. Sci. Semicond. Process., vol. 79, pp. 7–13, 2018.

[49] S. K. Panda, S. Chakrabarti, A. Ganguly, and S. ChLidhuri, "Photoluminescence and Raman study of CdS–Al2O3 nanocomposite films prepared by sol-gel techniques," J. Nanosci. Nanotechnol., vol. 5, pp. 459–465, 2005.

[50] S. S. Chiad, H. A. Noor, O. M. Abdulmunem, and N. F. Habubi, "Optical and structural properties of Ni-doped Co3O4 nanostructure thin films via CSPM," J. Phys.: Conf. Ser., vol. 1362, no. 1, 2019.

[51] Mártil de la Plaza, G. González-Díaz, F. Sánchez-Quesada, and M. Rodríguez-Vidal, "Structural and optical properties of r.f.-sputtered CdS thin films," Thin Solid Films, vol. 120, pp. 31–36, 1984.

[52] R. Bairy, J. A., G. K. Shivakumar, S. D. Kulkarni, R. Shivaraj, and P. S. Patil, "Effect of aluminium doping on photoluminescence and third-order nonlinear optical properties of nanostructured CdS thin films for photonic device applications," Physica B: Condens. Matter, vol. 555, pp. 145–151, 2019.

[53] N. Y. Ahmed, B. A. Bader, M. Y. Slewa, N. F. Habubi, and S. S. Chiad, "Effect of boron on structural, optical characterization of nanostructured Fe2O3 thin films," NeuroQuantology, vol. 18, no. 6, pp. 55–60, 2020.

[54] S. Agrawal, A. Parveen, and A. Azam, "Microwave assisted synthesis of Co-doped NiO nanoparticles and its fluorescence properties," J. Lumin., vol. 184, pp. 250–255, 2017.

[55] M. Contreras, M. J. Romero, and R. Noufi, "Characterization of Cu(In, Ga)Se2 materials used in record performance solar cells," Thin Solid Films, vol. 511, pp. 5154, 2006.

[56] J. Han, C. Spanheimer, G. Haindl, G. Fu, V. Krishnakumar, J. Schaffner, C. Fan, K. Zhao, A. Klein, and W. Jaegermann, "Optimized chemical bath deposited CdS layers for the improvement of CdTe solar cells," Sol. Energy Mater. Sol. C, vol. 95, pp. 816–820, 2011.

[57] M. B. Jumaa, T. H. Mubarak, and A. M. Mohammad, "Study of the structural, magnetic and electrical properties of Co1.2Fe1.8O4 nanoferrites," AIP Conf. Proc., vol. 2475, 090014, 2023.

[58] A. Davis, K. Vaccaro, H. Dauplaise, W. Waters, and J. Lorenzo, "Optimization of chemical bath-deposited cadmium sulfide on InP using a novel sulfur pretreatment," J. Electrochem. Soc., vol. 146, no. 3, pp. 1046–1052, 1999.

[59] M. Ilieva, D. Dimova-Malinovska, B. Ranguelov, and I. Markov, "High temperature electrodeposition of CdS thin films on conductive glass substrates," J. Phys.: Condens. Matter, vol. 11, no. 49, pp. 10025–10031, 1999.

[60] A. Aschour, “Physical properties of spray pyrolysed CdS thin films,” Turk. J. Phys., vol. 17, no. 8, pp. 551–558, 2003.

[61] B. Pradhan, A. K. Sharma, and A. K. Ray, “Conduction studies on chemical bath deposition nanocrystalline CdS thin films,” J. Cryst. Growth, vol. 304, no. 2, pp. 388–392, 2007.

[62] R. Mariappan, V. Ponnuswamy, M. Ragavendar, D. Krishnamoorthi, and C. Sankar, “The effect of annealing temperature on structural and optical properties of undoped and Cu-doped CdS thin films,” Optik, vol. 123, pp. 1098–1102, 2012.

[63] A. Mazón-Montijo, M. Sotelo-Lerma, L. Rodríguez-Fernández, and L. Huerta, “AFM, XPS and RBS studies of the growth process of CdS thin films on ITO/glass substrates deposited using an ammonia-free chemical process,” Appl. Surf. Sci., vol. 256, pp. 4280–4287, 2010.

[64] M. Contreras, M. Romero, B. To, F. Hasoon, R. Noufi, S. Ward, and K. Ramanathan, “Optimization of CBD CdS process in high-efficiency Cu(In,Ga)Se2-based solar cells,” Thin Solid Films, vol. 403–404, no. 579, pp. 204–211, 2002.

[65] S. S. Chiad, H. A. Noor, O. M. Abdulmunem, N. F. Habubi, M. Jadan, and J. S. Addasi, “Optical and structural performance of nanostructured Te thin films by (CSP) with various thicknesses,” J. Ovonic Res., vol. 16, no. 1, pp. 35–40, 2020.

[66] L. I. Soliman, H. H. Afify, and I. K. Battisha, “Growth impedence of pure CdS films,” Indian J. Pure Appl. Phys., vol. 42, pp. 12–17, 2004.

[67] Herrera-Molina, J. E. Diosa, A. Fernández-Pérez, and E. Mosquera-Vargas, “Influence of aluminum doping on structural, morphological, vibrational, and optical properties of CdS thin films obtained by chemical bath deposition,” Mater. Sci. Eng. B, vol. 273, 115451, 2021.

[68] Z. L. Raza Khan, M. Anver Aziz, and M. Shahid Khan, “Sol-gel derived CdS nanocrystalline thin films: optical and photoconduction properties,” Mater. Sci. Poland, vol. 36, pp. 235–241, 2018.

[69] J. I. Pankove, Optical Processes in Semiconductors, 6th ed., Prentice-Hall, New Jersey, pp. 6, 11, 1971.